Chemical Science

ROYAL SOCIETY OF CHEMISTRY

EDGE ARTICLE

View Article Online
View Journal | View Issue

Open Access Article. Published on 13 March 2023. Downloaded on 2/7/2026 7:50:00 PM.
This article is licensed under a Creative Commons Attribution-NonCommercial 3.0 Unported Licence.

Check for updates

Cite this: *Chem. Sci.*, 2023, **14**, 3852

All publication charges for this article have been paid for by the Royal Society of Chemistry

PyrroTriPol: a semi-rigid trityl-nitroxide for high field dynamic nuclear polarization†

Thomas Halbritter,‡[a] Rania Harrabi,‡[b] Subhradip Paul,[b] Johan van Tol,[c] Daniel Lee,[bd] Sabine Hediger,[b] Snorri Th. Sigurdsson,*[a] Frédéric Mentink-Vigier*[c] and Gaël De Paëpe*[b]

Magic angle spinning (MAS) dynamic nuclear polarization (DNP) has significantly broadened the scope of solid-state NMR to study biomolecular systems and materials. In recent years, the advent of very high field DNP combined with fast MAS has brought new challenges in the design of polarizing agents (PA) used to enhance nuclear spin polarization. Here, we present a trityl-nitroxide PA family based on a piperazine linker, named PyrroTriPol, for both aqueous and organic solutions. These new radicals have similar properties to that of TEMTriPol-I and can be readily synthesized, and purified in large quantities thereby ensuring widespread application. The family relies on a rigid bridge connecting the trityl and the nitroxide offering a better control of the electron spin–spin interactions thus providing improved performance across a broad range of magnetic fields and MAS frequencies while requiring reduced microwave power compared to bis-nitroxides. We demonstrate the efficiency of the PyrroTriPol family under a magnetic field of 9.4, 14.1 and 18.8 T with respect to TEMTriPol-I. In particular, the superiority of PyrroTriPol was demonstrated on γ-Al_2O_3 nanoparticles which enabled the acquisition of a high signal-to-noise surface-selective ^{27}Al multiple-quantum MAS experiment at 18.8 T and 40 kHz MAS frequency.

Received 24th October 2022
Accepted 12th March 2023

DOI: 10.1039/d2sc05880d

rsc.li/chemical-science

1 Introduction

Over the past decade, dynamic nuclear polarization (DNP) has emerged as a powerful technique to increase the sensitivity of solid-state magic angle spinning (MAS) NMR by transferring polarization from unpaired electrons to the nuclei of the substrate of interest.[1–6] In the case of exogeneous DNP, the sample is doped with a small paramagnetic molecule, referred to as a polarizing agent (PA), and the sample is irradiated with microwaves (μw) during signal acquisition.[2,4–8] Polarization transfer results in a substantial increase in sensitivity, *e.g.* with a theoretical enhancement of ^{1}H ∼ 658 and ^{13}C ∼ 2633, enabling new insights into structure and function in biology[9–16] and materials.[3–5,17–20]

Several DNP mechanisms have been proven to be active under MAS at high magnetic field (>5 T), namely the solid effect (SE), the Overhauser effect (OE) and the cross effect (CE). CE is to date the most efficient mechanism in terms of returned sensitivity at high magnetic fields (>10 T) using continuous μw irradiation.[7,8,21–25] The ideal PA for CE should consist of two coupled unpaired electrons, each of which should have a sharp-line electron paramagnetic resonance (EPR) spectrum, separated by the Larmor frequency of the nucleus of interest.[23,26,27] However, such ideal radical pairs are currently not known. Therefore, an extended effort has been made in the last two decades to synthesize improved PAs for MAS-DNP.

The quest started in 2003 with the introduction of the first broad-line bis-nitroxides by Griffin and coworkers.[7] The biradical structures were subsequently optimized and nowadays efficient PAs include AMUPol,[28] TEKPol,[29] bcTol(-M),[30,31] and more recently TinyPol[32] and (c)AsymPol-POK.[33,34]

Hetero-biradicals containing overlapping narrow and broad EPR lines, such as TEMTriPol-I[35,36] and HyTEK(-2),[37] were introduced to overcome the drawbacks of bis-nitroxides, such as AMUPol and TEKPol,[28,29] that exhibit a decreased CE-DNP efficiency at very high field (>10 T) and fast MAS (>15 kHz).[35–38] These hetero-biradicals require lower μw field to saturate one of the electron spin transitions as compared to nitroxides, which possess broader EPR lines that are harder to saturate.[39,40] This results in easier creation of a polarization difference between the two electrons, hence, better CE efficiency.[23,39] There is thus a clear relevance to develop further hetero-biradicals, especially for either low power μw sources or high field and fast MAS applications.

[a]Department of Chemistry, University of Iceland, Science Institute, Dunhaga 3, 107 Reykjavik, Iceland. E-mail: snorrisi@hi.is

[b]IRIG, MEM, Univ. Grenoble Alpes, CEA, CNRS, 38000 Grenoble, France. E-mail: gael.depaepe@cea.fr

[c]National High Magnetic Field Laboratory, Florida State University, Tallahassee, FL 32310, USA. E-mail: fmentink@magnet.fsu.edu

[d]Department of Chemical Engineering, University of Manchester, Manchester, M13 9PL, UK

† Electronic supplementary information (ESI) available. See DOI: https://doi.org/10.1039/d2sc05880d

‡ These authors contributed equally.

© 2023 The Author(s). Published by the Royal Society of Chemistry

Open Access Article. Published on 13 March 2023. Downloaded on 2/7/2026 7:50:00 PM.
This article is licensed under a Creative Commons Attribution-NonCommercial 3.0 Unported Licence.

The DNP mechanisms under MAS can be understood through numerical simulations that describe a series of discrete events that occur periodically within one rotor period.[22,23] These "rotor events"[39] correspond to fast energy-level anti-crossings[22,23] and can be classified in four categories: first, the μw rotor events that induce a change in the electron polarization; second, the electron dipolar–*J* (exchange) rotor events that tend to swap the electron polarization; third, the cross-effect rotor events (CE) that exchange part of the electron polarization difference with the nuclear polarization of the hyperfine coupled nuclei; fourth, the nuclear dipolar rotor events that enable the spin diffusion from the close protons to ones further away. It is worth noting that the performance drop of bis-nitroxides at high magnetic field and fast MAS, can be mitigated, in part, using structures with large enough electron–electron (e–e) spin couplings (dipolar $D_{a,b}$ and $J_{a,b}$ exchange interaction) and suitable relative *g*-tensor relative orientation.[33,40–42] This was first demonstrated with the introduction of the AsymPol biradical family, which yields short buildup times and excellent DNP efficiency defined as $\varepsilon_B/\sqrt{T_B}$ with ε_B defined as the signal gain with μw compared to the thermal equilibrium signal (not the signal in the absence of μw).[33] These radicals can very efficiently polarize proton-dense systems, including at high fields and fast MAS.[33,34] Yet, a performance drop in larger diameter MAS rotors (*e.g.* 3.2 mm, sapphire) is still observed above 14.1 T.[33,34]

In recent years, two organic radicals with relatively narrow EPR lines have been included in new biradical PAs for DNP, first the Finland trityl[35,43] and second 1,3-bis(diphenylene)-2-phenylallyl (BDPA).[37] For water-based applications, the trityl-nitroxide TEMTriPol-I,[35] and the hydrophilic NATriPol derivatives[43] have been shown to exhibit good performance at high magnetic fields. The solubility and the DNP performance were further improved by replacing the Finland trityl by its hydrophilic derivatives OX063 which led to the development of the SNAPol biradical.[44] These PAs appear promising but are not commercially available yet. One of the limiting factors might be their relatively challenging preparation. For instance, the synthesis of TEMTriPol-I involves a difficult and time-consuming HPLC purification step, which lead to low yield in our hands.

For organic solvents, HyTEK-2,[37] a BDPA-nitroxide, has recently been reported as an efficient polarizing agent with DNP enhancement factors of up to 200 and a buildup time of 8 s using a 32 mM radical concentration in a 0.7 mm rotor at 21.1 T.[45] A major drawback of BDPA-based biradicals is their limited solubility in aqueous solutions and apparent low persistence even in organic solvents,[37,45–49] although new BDPA derivatives with improved properties have recently been reported.[48] Trityl-nitroxide structures for organic solvents were also prepared and generated enhancements of ≈50 using 15 mM solution, however their performance was only assessed at 9.4 T.[50,51]

Here we introduce a new trityl-nitroxide family, dubbed PyrroTriPol, that can be used in aqueous and non-aqueous based media. We show that these new PAs are very efficient especially at high magnetic and fast MAS and that they also require ∼2–3 times less microwave power than bis-nitroxides. The new PA family was designed with a rigid piperazine linker and a pyrrolinoxyl radical. The carbon–carbon double bond from the five membered ring radical is conjugated with the carbonyl group from the linker and we demonstrate that it improves the stiffness of the linker. The main goal was to restrict the distribution of conformations that is typically encountered with flexible linkers (*e.g.*, TEMTriPol-I), to limit the presence of too large e–e couplings, since it can lead to inefficient CE rotor events.[22,23,39,40] Furthermore, this new biradical can be synthesized with high yield and is easily purified. The latter point is important since an upscale of the synthesis of such compounds can be envisioned readily, will ensure widespread application.

The MAS-DNP enhancement, buildup time, and overall sensitivity were evaluated for PyrroTriPol and PyrroTriPol-OMe at various magnetic fields (9.4, 14.1, 18.8 T), and compared with TEMTriPol-I, one of the best biradicals for aqueous solution, and a modified version (TEMTriPol-OMe), soluble in organic solvents (Fig. 1). Overall, we demonstrate that these biradicals exceed the performance of TEMTriPol-I in water-based matrices and TEMTriPol-I-OMe, the organic solvent version of TEMTriPol-I, in organic solvent. As a demonstration of high performance, we report a record enhancement at 18.8 T and 40 kHz MAS frequency with PyrroTriPol-OMe, which reaches 150 with a buildup time of 3.2 s in organic solvent using a biradical concentration of only 16 mM, and 90 for γ-alumina making it one of the best performing biradicals for high field MAS-DNP of materials.

2 Results and discussion

2.1 Bis-nitroxides *versus* hetero-biradicals for MAS-DNP

Bis-nitroxides have been actively developed in recent years to provide better performance than the first generation of biradicals.[28–34,52–55] Some of these PAs are attractive solutions since they can also be synthetized in large scale enabling a broader access to the community. In addition, recent structures with larger e–e couplings such as, AsymPol-POK/cAsymPol-POK and *m*-TinyPol[32–34] have partly mitigated the magnetic field and MAS dependency. For instance, it is worth pointing out that the Boltzmann enhancement factor ε_B for the AsymPol-POK biradicals is numerically predicted not to change significantly between 9.4, 14.1 and 18.8 T, at least not to the extent observed experimentally. Based on spin dynamics simulations performed with a fixed μw nutation field and

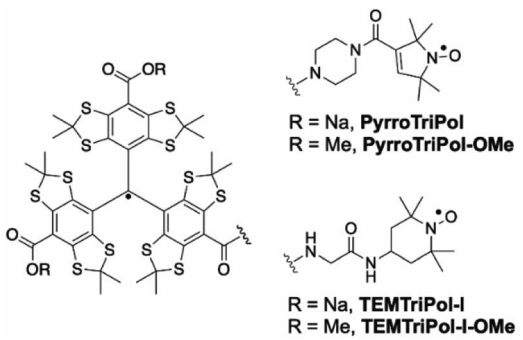

Fig. 1 Chemical structures of PyrroTriPol/TEMTriPol-I (for aqueous solution) and PyrroTriPol-OMe and TEMTriPol-I-OMe (for organic solutions).

Open Access Article. Published on 13 March 2023. Downloaded on 2/7/2026 7:50:00 PM.
This article is licensed under a Creative Commons Attribution-NonCommercial 3.0 Unported Licence.

spinning frequency, no drop is expected for AsymPol-POK.[33,34] This prediction held true when comparing 9.4 and 14.4 T experimental results obtained with the same diameter rotor (3.2 mm sapphire) for AMUPol, or AsymPol-POK,[34,56,57] but a clear drop of efficiency is observed when going to 18.8 T.[35,36,38,58] We, and others,[45,58] hypothesize that one of the reasons for the performance drop relates to the difficulty to produce large nutation frequency (>0.1 MHz) throughout the sample volume (inside NMR rotors) at very high magnetic fields (>18.8 T). This effect is directly related to μw absorption at submillimeter wavelength, where increased loss tangent coefficients imply reduced μw penetration depth[59,60] while increasing μw sample heating.[60] This effect is partly mitigated with the use of smaller diameter rotors (<3.2 mm), and this was asserted to explain the better DNP performance when using 1.3 and 0.7 mm rotors.[37,45,58]

In the case of hetero-biradicals, such as trityl-nitroxide or BDPA-nitroxide, the PAs possess one slowly relaxing electron spin with a narrow EPR line. This explains their moderate μw power requirement to generate efficient DNP. They also have some additional built-in features: the isotropic *g*-values of carbon and nitroxide radicals are approximately separated by the ^{1}H Larmor frequency,[27,35] leading to a much lower or even non-existing depolarization effect.[36] In addition, the presence of a narrow line improves the efficiency of all the rotor events, including the CE and dipolar/*J* rotor events efficiency for a given e–e coupling, magnetic field and spinning frequency.[36]

2.2 Design of a new trityl-nitroxide with a rigid bridge: the PyrroTriPol family

In the case of TEMTriPol-I, the presence of a broad distribution of e–e couplings was evidenced *via* high-field EPR at 100 K.[35,36,61] This broad distribution is likely due to the high flexibility of the TEMTriPol-I molecule which leads to multiple conformations, and thus a range of e–e couplings, at cryogenic temperatures. This feature was used to explain the relative robustness of the PA with respect to an increase of magnetic field, but also to highlight that a significant fraction of e–e couplings were too large to contribute to the CE mechanism, particularly at 9.4 T and even at 18.8 T.[36] Indeed, even if sizable e–e couplings $|D_{a,b} + 2J_{a,b}|$ a are helpful for the CE rotor events,[39,40] they should not exceed the Larmor frequency of the targeted nuclear spins.[25,33,35,36]

Based on this analysis, we explored the case of a more rigid bridge based on a piperazine linker.

Fig. 1 shows the structure of TEMTriPol-I and PyrroTriPol. The piperazine bridge chosen for PyrroTriPol is rigid due the presence of the 6 membered ring as well as the conjugation of the amide and the double bond present on the 5 membered nitroxide ring.[33] The radical–radical distance in PyrroTriPol and TEMTriPol-I, in their extended conformations, are nearly identical (around 14.6–14.9 Å).

2.3 Synthesis procedure

Nitroxide **3** and piperazine were connected through a peptide linkage to give **4**, and subsequent coupling reaction with trityl radical **5**[62,63] to form PyrroTriPol-OMe (Scheme 1). Saponification of PyrroTriPol-OMe yielded the water-soluble biradical PyrroTriPol (Scheme 1). Similarly, we prepared TEMTriPol-I[36] and its methyl ester derivatives TEMTriPol-I-OMe. The synthesis started by deprotection of boc-glycine-TEMPO **1**, followed by peptide coupling with trityl radical **5** to form TEMTriPol-I-OMe. Hydrolysis of the esters of TEMTriPol-I-OMe yielded TEMTriPol-I. Details regarding the synthesis can be found in the ESI,† but from Scheme 1, it is clear that PyrroTriPols give higher yield.

2.4 Density functional theory and molecular dynamics calculations

The bridge designed for PyrroTriPol was subjected to a theoretical analysis based on Density Functional Theory (DFT), followed by Molecular Dynamics (MD) calculations. These calculations were conducted to assess the conformation distribution of PyrroTriPol and the results were compared to those of TEMTriPol-I. The MD simulations were carried out in explicit glycerol/water mixture, to faithfully reproduce their behaviour, over 300 ns. The distance between the central carbon of the trityl and the middle of the NO bond of the nitroxides was measured and the corresponding histogram is reported in Fig. 2. The MD simulations predict a more rigid bridge for PyrroTriPol as compared to TEMTriPol-I. Indeed, the distribution of the distance for TEMTriPol-I is very broad, and extends between 8 and 15 Å, with a centre of mass located at 11 Å (corresponding to ∼39 MHz e–e dipolar coupling). In the case of PyrroTriPol, the distance distribution of PyrroTriPol is clearly bimodal. The main "mode", or the major conformer, corresponds to a conformation where the molecule is "extended" (see Fig. S1(c)†). The trityl-nitroxide distance spans 13.3 to 15 Å with

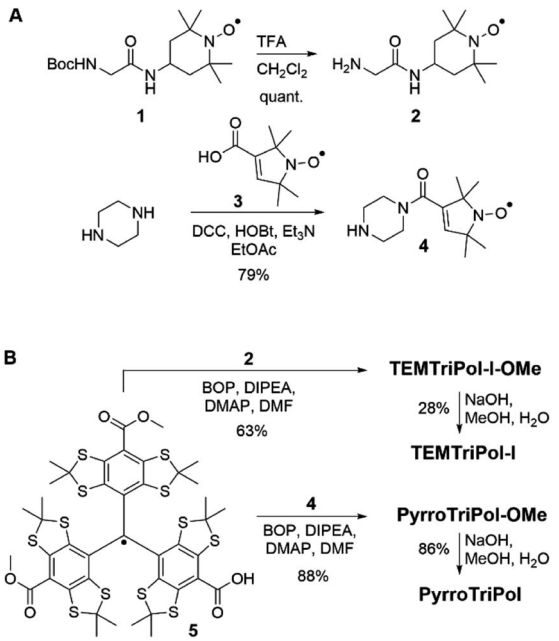

Scheme 1 Synthesis of the bi-radicals TEMTriPol-I, PyrroTriPol, TEMTriPol-I-OMe, and PyrroTriPol-OMe.

 © 2023 The Author(s). Published by the Royal Society of Chemistry

Open Access Article. Published on 13 March 2023. Downloaded on 2/7/2026 7:50:00 PM.
This article is licensed under a Creative Commons Attribution-NonCommercial 3.0 Unported Licence.

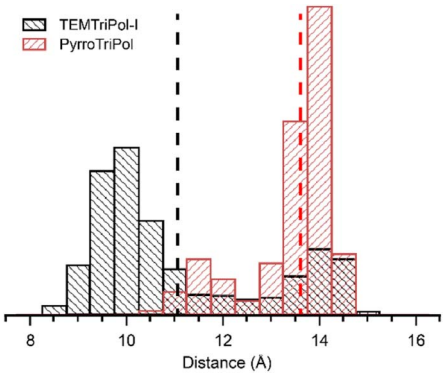

Fig. 2 Distribution of the distance between the central carbon of the trityl and the nitroxide extracted from MD simulations for PyrroTriPol (red, right leaning diagonals) and TEMTriPol-I (black, left leaning diagonals); vertical lines indicate the mean value of the distributions.

an average value at 13.7 Å ($D_{a,b} \sim 20$ MHz). The other mode represents a minor conformer where the molecule is "contracted" (see Fig. S1(d)†), with an average trityl-nitroxide distance of 11.5 Å ($D_{a,b} \sim 35$ MHz).

2.5 MAS-DNP field sweep profiles and exchange distribution

To confirm the prediction, the DNP-enhanced ssNMR signal was measured as a function of the magnetic field at both 9.4 and 14.1 T, for a fixed μw frequency for both water-soluble PyrroTriPol and TEMTriPol-I (Fig. 3).

At first sight, we note that the largest enhancement is observed at a positive optimum around 9.402 and 14.099 T, for both TEMTriPol-I and PyrroTriPol. These field positions correspond to the approximate on-resonance irradiation of the trityl moiety. At the low-field side, the DNP enhancement is negative and much smaller than the positive maximum for both PyrroTriPol and TEMTriPol-I. Importantly, the MAS-DNP field profiles differ around the maximum positive enhancement: this maximum is sharp and symmetric in the case of PyrroTriPol. In the case of TEMTriPol-I, the field profile presents a shoulder next to the optimal positive enhancement, in perfect agreement with previously reported data and thereby confirming the reproducibility of this behavior.[36]

As detailed in our previous work,[36] the relatively broad positive maximum for TEMTriPol-I implies the presence of a broad distribution of e–e couplings (dipolar, $D_{a,b}$, and exchange, $J_{a,b}$). The absence of a shoulder in the PyrroTriPol case proves that the semi-rigid linker clearly mitigates the presence of these large e–e couplings. This result is fully consistent with the DFT/MD simulations that predict a narrow distribution of average dipolar couplings around 20 MHz in the case of PyrroTriPol.

To confirm these predictions, we measured the EPR spectra of TEMTriPol-I and PyrroTriPol at 240 GHz (see Fig. S2†). The EPR spectrum of PyrroTriPol can be fitted using the two conformers that were extracted from the MD simulations. The main component of the EPR spectrum, 80%, arises from the "extended" conformer of PyrroTriPol (Fig. S1(c)†) which

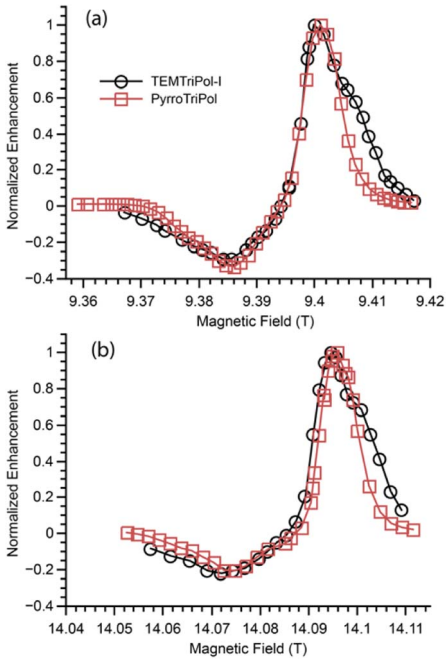

Fig. 3 Experimental MAS-DNP field profiles for PyrroTriPol (red squares) and TEMTriPol-I (black circles) at 10 mM radical concentration, in d_8-glycerol/D_2O/H_2O (60 : 30 : 10; v/v/v) at magnetic fields (μw frequencies/^{1}H Larmor frequency) of (a) 9.4 T (263.67 GHz/400 MHz) and (b) 14.1 T (395.45 GHz/600 MHz).

possesses a dipolar coupling $D_{a,b} \approx 25$ MHz and an exchange interaction $J_{a,b} \approx -8$ MHz. The minor component relates to the contracted conformer (Fig. S1(d)†), it represents 20% of the signals and possesses a dipolar coupling $D_{a,b} \approx 43$ MHz and an exchange interaction $J_{a,b} \approx -35$ MHz. An attempt to fit TEMTriPol-I with only two conformers (extended and contracted, see Fig. S1(a and b)†) was carried out. The fit yields a ratio 1 : 1 of these conformers but the agreement with the experimental spectra is arguable; it nonetheless confirms that TEMTriPol-I is flexible, and a significant portion of the conformers have large e–e couplings as previously discussed.[35,36] Since this biradical is flexible, the fit is an ill-posed problem as we would attempt to fit a distribution of dipolar couplings, exchange interactions, and relative orientation all at once.

As shown below, the presence of relatively smaller but sizeable e–e couplings in the case of PyrroTriPol ensures that all the trityl-nitroxide conformations can be saturated efficiently using a single μw irradiation frequency at the magnetic field of 9.4 T and above.

2.6 Microwave power dependence

One of the key strengths of hetero-biradicals such as trityl-nitroxide or BDPA-nitroxide is in the fact that the longitudinal relaxation times, $T_{1,e}$, of the trityl and BDPA are significantly longer than those of the nitroxides. They can be longer by one to two orders or magnitude at 100 K.[64,65] When the g-tensor interaction dominates the EPR spectrum, its stochastic

Open Access Article. Published on 13 March 2023. Downloaded on 2/7/2026 7:50:00 PM.
This article is licensed under a Creative Commons Attribution-NonCommercial 3.0 Unported Licence.

modulation through the Raman process is the dominant mechanism for relaxation, and since both BPDA and trityls have smaller *g*-anisotropy, *i.e.* smaller spin–orbit coupling, their relaxation times are longer.[64,66,67] The narrower linewidth also implies that the μw rotor events are more efficient when irradiating the narrow line radical.[36] In addition, for a given magnetic field, MAS frequency and e–e couplings, CE and dipolar–*J* rotor events are favored thanks to the presence of the narrow line radical. This was used to explain the high DNP efficiency of TEMTriPol-I and the relatively low power/μw nutation frequency requirement.[36]

The μw power dependency for PyrroTriPol and PyrroTriPol-OMe was measured at both 9.4 and 14.4 T using a 3.2 mm sapphire rotor. The 14.1 T instrument is equipped with a quasi-optic bench, which enables continuous variation the μw power from 0 to 12 W using a polarization grid while maintaining the gyrotron's parameters constant. The power was measured with an Ophir pyrometer 3A-P-THz and it was calibrated using a water load placed after the tapper that reduces the beam from 16 to 7.6 mm (see ESI Fig. S5†).[68] In this setup, the power read corresponds to the beam power propagating inside the probe's waveguide. Fig. 4 reports the normalized enhancement measured at the maximum field position, for PyrroTriPol, PyrroTriPol-OMe, TEMTriPol-I-OMe and TEKPol at 14.1 T. Each of the trityl-nitroxides have an optimal μw power of 4–6 W. In contrast, TEKPol requires more than 11 W to reach its optimum. We also note that the optimal μw power for PyrroTriPol and PyrroTriPol-OMe is lower than for TEMTriPol-I-OMe. This may be because the trityl linewidth is not broadened by the exchange interaction, slightly improving the efficiency of the μw rotor events as compared to the TEMTriPol-I-OMe.

Similar experiments were carried at 400 MHz/263 GHz. The μw power was calibrated at the probe base (using a water load before the tapper) and adjusted by varying the collector current, covering 8 to 22 W approximately. In this setup the power corresponds to what propagates into the 19 mm overmoded waveguide. The effective power at the sample is estimated to be 2 to 4 times smaller. In the case of bis-nitroxides (AMUPol/AsymPol-POK), a steady improvement is seen up to the maximum gyrotron output power, whereas less than a third of that power is already sufficient to saturate TEMTriPol-I and PyrroTriPol. At this stage, it is worth noting that 400 MHz/263 GHz Bruker gyrotrons operating in its fundamental mode have an overmoded HE11 Gaussian beam output with >90% purity and that each waveguide connection and miter bend can further introduce mode "impurities".[69,70] These mode impurities contribute to the power measured (calorimetric detection) although they are not useful for DNP and are in part reflected by the tapper. This problem is less present in the case of the second harmonic gyrotron operating at 395 GHz which produces high quality Gaussian beams[71] especially combined with the quasi-optic bench. Indeed a back-to-back horn does not improve the beam purity.[68]

The beam quality is improved when using klystrons (<5 W)[69,72,73] and solid-state sources (<500 mW),[70,74,75] that have been recently introduced for DNP experiments at 263 GHz. As a consequence, these power-limited sources are more efficient than gyrotrons in the low power range, so it will be very interesting to test them with polarizing agents such as PyrroTriPol.[69,70,72,74] For instance, simulations can predict the power dependence at 14.1 T for both PyrroTriPol-OMe and TEKPol (see Fig. S7(a)†). Using the same parameters, the simulations predict that a 500 mW solid-state source should be able to provide about half the sensitivity obtained with a gyrotron at 9.4 T/263 GHz in a 3.2 mm rotor (Fig. S7(b)†).

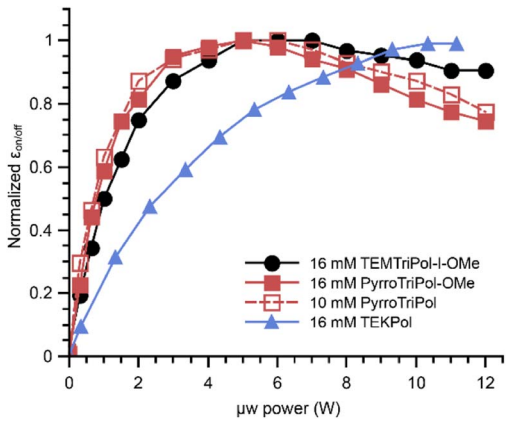

Fig. 4 Experimental μw power dependence of the normalized enhancement measured at 14.1 T, 8 kHz MAS frequency and ~100 K as a function of the μw power at the probe base for 10 mM PyrroTriPol in d_8-glycerol/D_2O/H_2O (60 : 30 : 10; % vol), (red open circle), 16 mM PyrroTriPol-OMe in 1,1,2,2-tetrachloroethane (TCE) (red circles), 16 mM TEMTriPol-I-OMe in TCE (black squares) and 16 mM TEKPol in TCE (blue diamonds). hBN was added to all the samples measured in TCE.

2.7 PyrroTriPol efficiency for frozen solutions at 9.4 and 14.1 T

The performance of PyrroTriPol, TEMTriPol-I, PyrroTriPol-OMe and TEMTriPol-I-OMe was assessed on frozen solutions at 9.4 and 14.1 T and 8 kHz MAS frequency. The aqueous glass-forming DNP matrix corresponds to a partially deuterated solution of d_8-glycerol/D_2O/H_2O (60 : 30 : 10; v/v/v) ([^{1}H] = 11 M, biradical concentration 10 mM) containing 0.25 M U–^{13}C,^{15}N-L-proline. In the case of the organic solvent, a 1,1,2,2-tetrachloroethane (TCE) solution ([^{1}H] = 18 M, biradical concentration 16 mM) was used to impregnate hBN particles to improve the quality of the glass, the μw penetration and the reproducibility of the results.[76,77] The returned sensitivity, depolarization, ε_{Depo}, DNP enhancement factor, $\varepsilon_{on/off}$, and buildup time, T_B, are presented in Fig. 5.

The first noticeable point is that all trityl-tempo biradicals have very limited depolarization effect, with $\varepsilon_{Depo} \approx 0.9$–1 at both 9.4 T and 14.1 T. This result was expected and is in full agreement with previous work conducted on TEMTriPol-I,[36] which explained the limited depolarization effect of such hetero-biradicals and homo-biradicals with large *g*-tensor distance.[36,41]

The second point is that DNP buildup times, T_B, are similar for PyrroTriPol/TEMTriPol-I and PyrroTriPol-OMe/TEMTriPol-I-

 © 2023 The Author(s). Published by the Royal Society of Chemistry

Open Access Article. Published on 13 March 2023. Downloaded on 2/7/2026 7:50:00 PM.
This article is licensed under a Creative Commons Attribution-NonCommercial 3.0 Unported Licence.

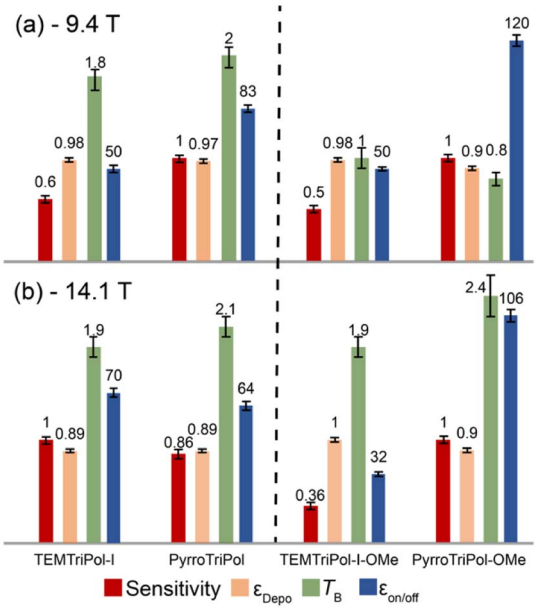

Fig. 5 Experimental relative sensitivity (red), ε_{Depo} (orange), T_B (green) and $\varepsilon_{on/off}$ (blue) measured for 10 mM TEMTriPol-I and PyrroTriPol in d_8-glycerol/D_2O/H_2O (60 : 30 : 10, %vol) containing 0.25 M of U–^{13}C,^{15}N-proline, 16 mM TEMTriPol-I-OMe and PyrroTriPol-OMe in TCE with hBN. The MAS frequency was 8 kHz and the temperature was ~110 K at 9.4 T (a) and 100 K at 14.1 T (b) and the ^{13}C signals after ^{1}H was measured.

OMe respectively. The relatively fast buildup times are the consequence of efficient *D*/*J* rotor events, due to the presence of a narrow line radical and of sufficient e–e couplings. Although TEMTriPols have, on average, larger e–e couplings than PyrroTriPols, it only translates into a slightly shorter buildup time. This can, in part be explained by the fact that couplings present in PyrroTriPol are sufficient to ensure efficient *D*/*J* and CE rotor events (given the presence of a narrow line radical) and that some of the couplings present in TEMTriPol-I are too large to contribute to the CE (especially at low magnetic field).

The biradicals are thus similar with regards to depolarization and buildup times, however they differ more significantly when considering the hyperpolarization performance.

The performance of PyrroTriPol-OMe in organic solvent-based DNP matrix is strikingly high (Fig. 5). At 9.4 T it returns a record $\varepsilon_{on/off} \approx 120$, significantly larger than alternate trityl-nitroxide structures previously reported,[50,78] while TEMTriPol-I-OMe reaches an enhancement factor $\varepsilon_{on/off} \approx 50$. Since depolarization and buildups are nearly equivalent, this translates into a ×2.4 improvement in sensitivity compared to TEMTriPol-I-OMe. At higher magnetic field of 14.1 T, the performance contrast between the PyrroTriPol-OMe and TemTriPol-I-OMe is even larger. PyrroTriPol-OMe yields $\varepsilon_{on/off} \approx 106$ while TEMTriPol-I-OMe stalls at 32. This means that PyrroTriPol-OMe improves the sensitivity by a factor ~2.5 at 14.1 T, relative to TEMTriPol-I-OMe. Additional experiments on PyrroTriPol-OMe and TEMTriPol-OMe were carried out using a 10 mM biradical concentration. In that case, the enhancement of PyrroTriPol-OMe is unchanged while it slightly increases for TEMTriPol-OMe from 32 to 44. In both cases, the buildup times become longer: 3.5 and 3.8 s respectively. These additional experiments indicate that TEMTriPol-OMe aggregates in TCE while PyrroTriPol-OMe remains well solubilized.

It is also interesting to note that PyrroTriPol-OMe in TCE consistently returns higher DNP enhancement factor than PyrroTriPol in glycerol/water. At 9.4 T, PyrroTriPol yields relatively high DNP enhancement factor ($\varepsilon_{on/off} \approx 80$), higher than TEMTriPol-I ($\varepsilon_{on/off} \approx 50$, in agreement with ref. 36). The higher $\varepsilon_{on/off}$, yet similar depolarization and buildup, results in higher polarization gain that makes the resulting sensitivity 1.6 times higher for PyrroTriPol than TEMTriPol-I. We note that at 14.1 T, the results appear at first slightly less favorable to PyrroTriPol compared to TEMTriPol-I. Since the structure of PyrroTriPol-OMe and PyrroTriPol are very similar, we believe that this could arise from the limited solubility of PyrroTriPol and/or its tendency to aggregate. To illustrate this point, we have recorded the concentration dependency for PyrroTriPol (ESI Table S2†). Higher DNP enhancement factors can be obtained at lower PA concentration: ~105 at 3 mM, ~80 at 5 mM and ~74 at 10 mM, but with longer recycling time. The latter point is not surprising but the increase in DNP enhancement factor while lowering the concentration is unusual. This indicates that PyrroTriPol, like TEMTriPol-I,[43] has a propensity to aggregate in water-based glass matrices and this was partially confirmed by EPR (see Fig. S4†). For this reason, we are currently developing a PyrroTriPol derivative with higher aqueous solubility. We expect that this new version should provide DNP enhancement factors >100 at relatively high radical concentration (up to 40 mM).

2.8 Trityl-nitroxide biradicals *versus* triradicals

Thanks to the high yielding PyrroTriPol synthesis, the performance of the trityl-nitroxide biradical was also compared to a triradical, containing one trityl and two or three nitroxides. This topic was recently addressed by Li *et al.*[79] and one of the explored hypotheses is that increasing the number of nitroxides moieties should improve the DNP performance. Since PyrroTriPol-OMe performed well in TCE, without showing signs of aggregation, we thus synthesized the triradical version, dubbed DiPyrroTriPol-OMe, which was compared to TEMTriPol-I-OMe and DiTEMTriPol-I-OMe (Fig. 6(a)).

The performance of these triradicals at 9.4 and 14.1 T is shown in Fig. 6(b). Overall, the performance is similar or lower than their biradical counterparts for a fixed electron concentration. At 11 mM, DiPyrroTriPol-OMe performs reasonably well ($\varepsilon_{on/off} \approx 73$ and 78 at 9.4 and 14.1 T, respectively) but is less efficient than 10 mM or even 16 mM PyrroTriPol-OMe because of slower DNP build up times ($T_B = 1.8$ and 3.8 s at 9.4 T and 14.1 T for 10 mM). In the case of DiTEMTriPol-I-OMe, the DNP performance are clearly drops with $\varepsilon_{on/off} \approx 20$ and 16 at 9.4 and 14.1 T, respectively.

As such, this first experimental dataset does not verify the previously developed hypothesis: chemically tethering two or three nitroxide to a trityl does not necessarily enhance $\varepsilon_{on/off}$ or shorten the buildup time T_B. This seems to indicate that special

Open Access Article. Published on 13 March 2023. Downloaded on 2/7/2026 7:50:00 PM.
This article is licensed under a Creative Commons Attribution-NonCommercial 3.0 Unported Licence.

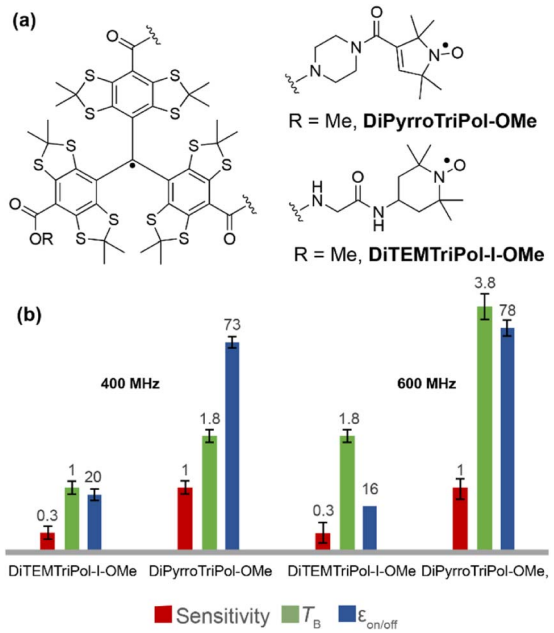

Fig. 6 (a) Chemical structures of DiPyrroTriPol-OMe/DiTEMTriPol-I-OMe for organic solutions, (b) experimental sensitivity, buildup time, and enhancement measured at 9.4 T and 14.1 T and 8 kHz MAS frequency, at 11 mM concentration in TCE with hBN.

conditions are required; not all triradicals made of two nitroxides and one trityl may outperform their biradical counterparts and special design may be required.

Fig. S7† shows MAS-DNP simulations[26] performed on spin systems mimicking PyrroTriPol-OMe (2 electrons – 1 proton) and DiPyrroTriPol-OMe (3 electrons – 1 proton). Interestingly, we observe a very different behaviour depending on whether the proton is coupled to the trityl or to one of the nitroxides. If the proton is linked to the trityl, the simulations show an increase in the DNP enhancement factor for the tri-radical. This can be qualitatively rationalized by arguing that the proton undergoes (on average) twice as many CE rotor events. In this situation, one would expect a shorter buildup time in the case of a tri-radical. In the case when the proton is coupled to one of the nitroxides, the simulations show a similar DNP enhancement factor (ESI Fig. S7†). This result is valid as long as the hyperfine coupling to the second nitroxide can be neglected and if the nitroxide–nitroxide coupling is weak. In real systems, the situation is very different from these two ideal cases. First, there is more than one proton contributing. Second, the strongly coupled protons are mostly present on the nitroxides and not on the trityl moieties. Finally, one cannot rule out the presence of non-negligible nitroxide–nitroxide couplings (both intra and intermolecular) that would decrease the overall efficiency. All in all, this can tentatively explain why we observe experimentally a decrease of the DNP enhancement factor and a lengthening of the buildup time in the case of DiPyrroTriPol-OMe *versus* PyrroTriPol-OMe. In addition, one cannot exclude that the triradicals may be more prone to aggregation.

2.9 MAS-DNP NMR on proton-dense molecular solids

As recently highlighted,[34] it is also important to benchmark PAs on proton-dense molecular solids. To that end, we choose two microcrystalline powders, cellulose and adenosine, to further investigate the performance of PyrroTriPol and TEMTriPol PAs. In each case, the proton density is relatively high (92 and 102 M, respectively). The overall sensitivity is consistently larger for the PyrroTriPol PAs compared to the TEMTriPol PAs (Fig. 7). In the case of cellulose (Fig. 7(a)), the sensitivity is ∼62 $s^{-1/2}$ for PyrroTriPol, which is ×1.4 higher than for TEMTriPol-I at a biradical concentration of 10 mM, corresponding to about a factor of ×2 in timesaving at 9.4 T. Similar conclusions can be drawn for adenosine (Fig. 7(b)), in which the PyrroTriPol-OMe and TEMTriPol-I-OMe are tested. Improvement of about a factor of ×2.2 for PyrroTriPol-OMe, translates into a timesaving of ×4.8.

2.10 MAS-DNP efficiency at very high field (18.8 T) and fast MAS (40 kHz)

The MAS-DNP performance of the PyrroTriPol family was also evaluated and compared to TEMTriPol-1 at high magnetic field (18.8 T) and fast MAS frequency (40 kHz) using a 1.3 mm DNP probe.

Due to limited access to instrument time, and the difficulty to assess the depolarization factor on a 1.3 mm probe compared to the probe background, it was not measured. Indeed, such measurements require to quantitatively measure the ^{1}H OFF signal (in the absence of microwave irradiation) under static and sample spinning conditions. With a 1.3 mm probe, the ^{1}H background of the probe can be substantial compared to the ^{1}H OFF signal which yields large error in the estimation of the depolarization factor. It is worth noting that recently contribution factors have been reported on a 1.3 mm probe.[37] Nevertheless such measurements cannot be used to access the ^{1}H depolarization factor directly since it relies on ^{13}C-detected experiments and would still require the measurement under

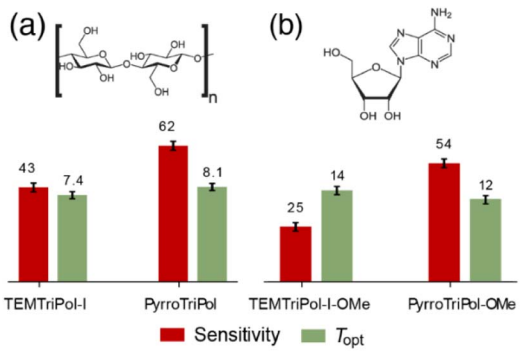

Fig. 7 Experimental sensitivity (red), optimal recycling delay for sensitivity, T_{opt}, as defined in ref. 34 and ESI† (green) measured for (a) cellulose microcrystalline powder impregnated with 10 mM TEMTriPol-I and PyrroTriPol in d_8-glycerol/D_2O/H_2O (60 : 30 : 10 v/v) and for adenosine microcrystalline powder impregnated with (b) 16 mM TEMTriPol-I-OMe and PyrroTriPol-OMe. All the data were recorded at 9.4 T, 8 kHz MAS and 110 K. Chemical structures of (a) cellulose and (b) adenosine are shown above the data plots.

 © 2023 The Author(s). Published by the Royal Society of Chemistry

Open Access Article. Published on 13 March 2023. Downloaded on 2/7/2026 7:50:00 PM.
This article is licensed under a Creative Commons Attribution-NonCommercial 3.0 Unported Licence.

static condition. As noted above, the depolarization effect is induced by sample spinning[80] and is radical-dependent.[81] If present, it typically manifests itself as a decrease of the ^{1}H polarization, compared to the static case, through a reverse CE mechanism in the absence of microwave irradiation. The drop in polarization as a function of MAS typically reaches a plateau at 1–10 kHz.[33,36,40,81] The magnitude is likely to stay constant or decrease at much higher spinning frequencies. This is illustrated with the simulations reported in Fig. S9.†

As a consequence, the DNP enhancement factor, buildup time, sensitivity and the $\varepsilon_{on/off}/\sqrt{T_B}$ are reported (Fig. 8). The DNP buildup times (T_B) at 18.8 T are longer than at lower field and lower MAS frequency. PyrroTriPol and TEMTriPol-I yield $T_B = 5$ s at 40 kHz and their organic solvent counterparts give $T_B = 4.5$ s for TEMTriPol-I-OMe, and 3.2 s for PyrroTriPol-OMe. Such an increase in buildup time is expected as the CE rotor events become less efficient. This is consistent with theoretical predictions[23,39,40,82] and previously reported experiments on bis-nitroxide, trityl-nitroxide and BDPA-nitroxide PAs.[35–37,45,83] More interestingly, the DNP enhancements are still high for PyrroTriPol and PyrroTriPol-OMe with $\varepsilon_{on/off} = 100$ and 150, respectively. For comparison, TEMTriPol-I and TEMTriPol-OMe give 68 and 50, respectively.

Overall, the sensitivity and $\varepsilon_{on/off}/\sqrt{T_B}$ confirm the improvements yielded by PyrroTriPol. Both are consistently larger than for TEMTriPol-I, with a factor of ×1.5 and ×2–3 for aqueous and organic solvents, respectively. The superiority of PyrroTriPol is again more pronounced in the case of organic solutions (PyrroTriPol-OMe), which is consistent with the results obtained at lower magnetic field and lower MAS frequency.

2.11 Application of PyrroTriPol-OMe at 18.8 T and 40 kHz MAS

Over the last decade, MAS-DNP has been proved extremely relevant to study the surface of materials,[76,84–87] including aluminas.[88–90] The approach often relies on polarizing the solvent protons by DNP before transferring the magnetization to near surface nuclei.[84] In the case of aluminas, the approach can be used to perform primostrato NMR studies of the various aluminium sites present in the first layer.[90] For quadrupolar nuclei, such ^{27}Al, there is a clear interest in performing these experiments at high magnetic field. Indeed, the second order quadrupolar broadening is inversely proportional to the magnetic field.

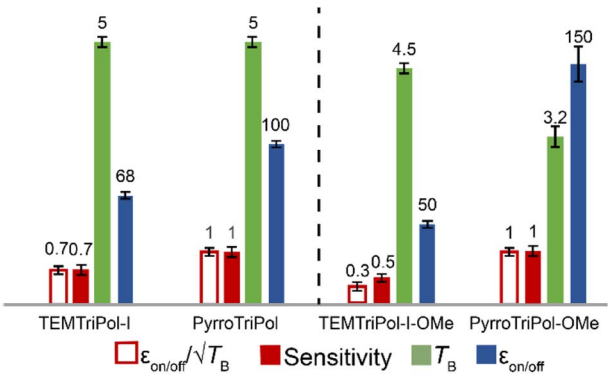

Fig. 8 Experimental performance of 10 mM PyrroTriPol and TEMTriPol-I in d_8-glycerol/D_2O/H_2O (60 : 30 : 10; v/v/v) containing 0.25 M of U–^{13}C,^{15}N-proline and 16 mM PyrroTriPol-OMe and TEMTriPol-I-OMe in TCE, at 18.8 T, 40 kHz MAS and ∼110 K. No hBN particules were added to the samples.

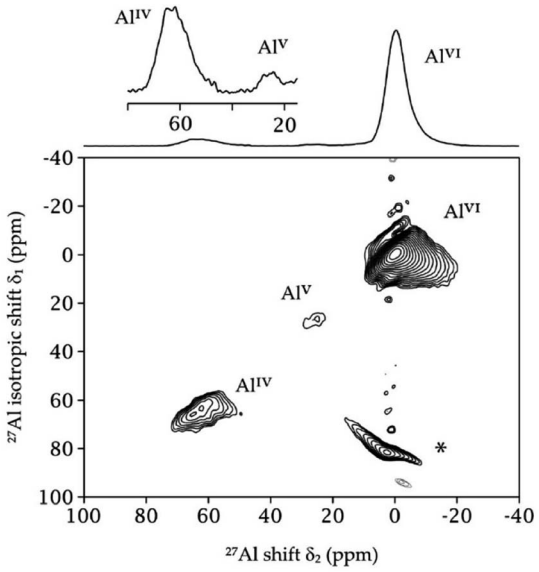

Fig. 9 Experimental DNP-enhanced ^{1}H–^{27}Al CP MQMAS NMR spectrum of γ-alumina nano-powder impregnated with 16 mM PyrroTriPol-OMe in TCE, recorded at 18.8 T, 40 kHz MAS frequency and ∼110 K, giving a DNP enhancement factor $\varepsilon_{on/off}$ ∼90. Spinning sidebands are indicated with a star.

Thanks to the excellent performance of PyrroTriPol-OMe in TCE, a primostrato {^{1}H–}^{27}Al Cross Polarization (CP) Multiple Quantum Magic Angle Spinning (MQMAS) 2D experiment[91,92] was performed on γ-alumina at 18.8 T and 40 kHz MAS using a non-aqueous impregnation. This is particularly relevant for the study of materials that are sensitive to water or air. This experiment (∼14 h) is presented in Fig. 9 and was made possible because of the excellent ^{1}H DNP enhancement factor ($\varepsilon_{on/off} \approx 90$) and with a buildup time of ∼9 s obtained with 16 mM PyrroTriPol-OMe in TCE. As a comparison, a ^{1}H DNP enhancement of 46 was reported with 32 mM HyTEK-2 in TCE using similar conditions (∼105–110 K, 40 kHz MAS, 800 MHz ^{1}H Larmor frequency).[37] This is a powerful illustration of the DNP efficiency of the newly-developed PyrroTriPol family, opening many perspectives to study different systems containing quadrupolar nuclei, where high field and fast MAS are required.

Conclusion and perspectives

We have introduced a new family of trityl-nitroxide PAs, dubbed the PyrroTriPol family, for both aqueous and organic solvents. This work was motivated by the need for improved PAs that can work efficiently at high magnetic field and fast MAS, soluble in

Open Access Article. Published on 13 March 2023. Downloaded on 2/7/2026 7:50:00 PM.
This article is licensed under a Creative Commons Attribution-NonCommercial 3.0 Unported Licence.

either water or organic solvent compatible systems. The work is built upon the ground-breaking TEMTriPol-I[35] and the fine understanding of its DNP mechanism.[36] TEMTriPol-I was the first biradical showing near field independent enhancements, and a very good performance at 18.8 T. In addition, it requires lower μw power (compared to bis-nitroxide PAs), does not generate depolarization and possesses significant e–e coupling, which enables fast buildup times.[36] However, its flexible linker yielded a distribution of large exchange interaction which are not all optimal for DNP. In addition, it was recently shown that it has the tendency to aggregate.[43] To overcome these limitations, we developed the PyrroTriPol family, which are based on a semi-rigid piperazine linker between the trityl and the nitroxide.

This linker provides more stiffness and reduces flexibility compared to TEMTriPol-I, which in turn reduces the number of accessible conformations and conserves optimal electron–electron interactions. This latter was demonstrated using MD simulations and manifested in the field profiles of both PyrroTriPol and TEMTriPol-I at 9.4 and 14.1 T. More importantly, we demonstrate that the specific EPR properties of the trityl radical exhibit higher DNP efficiency with less μw power, compared to bis-nitroxides. This is an important point since it partly mitigates the μw power loss encountered at high magnetic fields. As expected, the PyrroTriPol family exhibits in general a substantial improvement in MAS-DNP sensitivity when compared to TEMTriPol-derivatives at all applied magnetic fields and MAS frequencies, particularly for the organic solvent version. This is clearly pronounced in the case of PyrroTriPol-OMe, for which we obtain high DNP enhancement and short buildup time constants, even at 18.8 T and 40 kHz. This enables the recording of a CP MQMAS experiment at 18.8 T and 40 kHz on γ-Al_2O_3.

The water-soluble version presented in this work, *i.e.* PyrroTriPol, is mostly interesting for very high field application (where microwave losses are important) and for power-limited DNP experiments. At 9.4 and 14.4 T using a gyrotron as microwave source, PyrroTriPol does not outperform AsymPol-POK or cAsymPol-POK in the case where the sample does not absorb too much of the microwave. At 18.8 T, PyrroTriPol performs well, and seems to be competitive with the recently introduced SNAPols[44] and the very similar STAPols[93] that are geared towards in-cell DNP. We are currently developing a PyrroTriPol version with improved aqueous solubility that should help improving the results presented here.

Concerning PyrroTriPol-OMe (soluble in organic solvents), it is overall much better than TEKPol at all the experimental conditions tested in this work: 9.4/14.4/18.8 T up to 40 kHz MAS frequency. PyrroTriPol-OMe and HyTEK-2 are thus currently the two best performing PA for applications in organic solvent. A direct comparison with HyTEK-2 is not straightforward as both were tested under different concentrations. Nevertheless, both were tested on γ-Al_2O_3 at 18.8 T and 40 kHz MAS and PyrroTriPol-OMe returns higher DNP enhancement factor $\varepsilon_{on/off}$ with faster buildup time using reduced biradical concentrations.

In terms of perspective, we believe that the PyrroTriPol PAs have the potential to become broadly accessible to the DNP community. Indeed, the first two members introduced in this work (PyrroTriPol and PyrroTriPol-OMe) appear stable and straightforward to synthesize and purify, as compared to TEMTriPol-I. Thus, large scale synthesis can be envisioned.

In addition, the benefits of the PyrroTriPol PAs extend beyond the high field DNP realm since the μw power requirement is significantly lower than with bis-nitroxide PAs. This has significant implications as recent works have explored the use of lower power sources to provide more sustainable MAS-DNP solutions at 9.4 T using either extended interaction klystrons (EIKs) or solid-state sources.[70,74,94] The combination of these low power cost-effective sources and PyrroTriPol PAs is expected to enable a broader access to DNP.

Data availability

Data that support the findings of this study are available from the corresponding author upon reasonable request.

Author contributions

STS, FMV, and GDP designed and led the study. RH/SP/DL/SH, FMV, and GDP collected the NMR/DNP data at 9.4, 14.4, and 18.8 T. EPR data were collected by HVT. Simulations were performed by FMV and discussed with GDP as well as the other authors. TH synthesized the polarizing agent molecules under the guidance of STS. All authors contributed, through regular meetings, to the development of the project and the writing of the paper.

Conflicts of interest

There are no conflicts to declare.

Acknowledgements

This work was supported by the French National Research Agency (CBH-EUR-GS and Labex ARCANE ANR-17-EURE-0003, Glyco@Alps ANR-15-IDEX-02, and ANR-16-CE11-0030-03) and the European Research Council Grant ERC-CoG-2015 No. 682895 to G. D. P. Part of this work, carried out on the Platform for Nanocharacterisation (PFNC), was supported by the "Recherches Technologiques de Base" program of the French National Research Agency (ANR). This work was supported by the Icelandic Research Fund, Grant No. 173727, and the University of Iceland Research Fund (S. Th. S). T. H. thanks the Deutsche For-schungsgemeinschaft (DFG) for a postdoctoral fellowship (414196920). The National High Magnetic Field Laboratory (NHMFL) is funded by the National Science Foundation Division of Materials Re-search (DMR-1644779) and the State of Florida. A portion of this work was supported by the NIH P41 GM122698, NIH S10 OD018519 and from the European Union's Horizon 2020 Research and Innovation Programme under grant agreement no. 101008500. Financial support from the TGIR-RMN-THC Fr3050 CNRS for conducting DNP experiments at high magnetic fields (18.8 T) is gratefully

 © 2023 The Author(s). Published by the Royal Society of Chemistry

Open Access Article. Published on 13 March 2023. Downloaded on 2/7/2026 7:50:00 PM. This article is licensed under a Creative Commons Attribution-NonCommercial 3.0 Unported Licence.

acknowledged. FMV thanks Alexander Lomzov for his initial help with respect to trityl force-field.

References

1 L. R. Becerra, G. J. Gerfen, R. J. Temkin, D. J. Singel and R. G. Griffin, Dynamic nuclear polarization with a cyclotron resonance maser at 5 T, *Phys. Rev. Lett.*, 1993, **71**, 3561–3564.

2 A. B. Barnes, G. De Paepe, P. C. A. van der Wel, K.-N. Hu, C.-G. Joo, V. S. Bajaj, M. L. Mak-Jurkauskas, J. R. Sirigiri, J. Herzfeld, R. J. Temkin and R. G. Griffin, High-Field Dynamic Nuclear Polarization for Solid and Solution Biological NMR, *Appl. Magn. Reson.*, 2008, **34**, 237–263.

3 A. J. Rossini, A. Zagdoun, M. Lelli, A. Lesage, C. Copéret and L. Emsley, Dynamic nuclear polarization surface enhanced NMR spectroscopy, *Acc. Chem. Res.*, 2013, **46**, 1942–1951.

4 D. Lee, S. Hediger and G. De Paepe, Is solid-state NMR enhanced by dynamic nuclear polarization?, *Solid State Nucl. Magn. Reson.*, 2015, **66–67**, 6–20.

5 A. G. M. Rankin, J. Trébosc, F. Pourpoint, J.-P. Amoureux and O. Lafon, Recent developments in MAS DNP-NMR of materials, *Solid State Nucl. Magn. Reson.*, 2019, **101**, 116–143.

6 A. S. Lilly Thankamony, J. J. Wittmann, M. Kaushik and B. Corzilius, Dynamic nuclear polarization for sensitivity enhancement in modern solid-state NMR, *Prog. Nucl. Magn. Reson. Spectrosc.*, 2017, **102–103**, 120–195.

7 K.-N. Hu, H. Yu, T. M. Swager and R. G. Griffin, Dynamic Nuclear Polarization with Biradicals, *J. Am. Chem. Soc.*, 2004, **126**, 10844–10845.

8 S. Hediger, D. Lee, F. Mentink-Vigier and G. De Paëpe, MAS-DNP Enhancements : Hyperpolarization, Depolarization, and Absolute Sensitivity, *eMagRes*, WILEY-VCH Verlag, 2018, vol. 7.

9 T. Biedenbänder, V. Aladin, S. Saeidpour and B. Corzilius, Dynamic Nuclear Polarization for Sensitivity Enhancement in Biomolecular Solid-State NMR, *Chem. Rev.*, 2022, **122**, 9738–9794.

10 W. Y. Chow, G. De Paepe and S. Hediger, Biomolecular and Biological Applications of Solid-State NMR with Dynamic Nuclear Polarization Enhancement, *Chem. Rev.*, 2022, **122**, 9795–9847.

11 N. Ghassemi, A. Poulhazan, F. Deligey, F. Mentink-Vigier, I. Marcotte and T. Wang, Solid-State NMR Investigations of Extracellular Matrixes and Cell Walls of Algae, Bacteria, Fungi, and Plants, *Chem. Rev.*, 2022, **122**(10), 10036–10086.

12 D. Gauto, O. Dakhlaoui, I. Marin-Montesinos, S. Hediger and G. De Paëpe, Targeted DNP for biomolecular solid-state NMR, *Chem. Sci.*, 2021, **12**, 6223–6237.

13 S. Bahri, R. Silvers, B. Michael, K. Jaudzems, D. Lalli, G. Casano, O. Ouari, A. Lesage, G. Pintacuda, S. Linse and R. G. Griffin, 1 H detection and dynamic nuclear polarization–enhanced NMR of Aβ 1-42 fibrils, *Proc. Natl. Acad. Sci. U.S.A.*, 2022, **119**, e2114413119.

14 R. Ghosh, Y. Xiao, J. Kragelj and K. K. Frederick, In-Cell Sensitivity-Enhanced NMR of Intact Viable Mammalian Cells, *J. Am. Chem. Soc.*, 2021, **143**, 18454–18466.

15 P. Fricke, D. Mance, V. Chevelkov, K. Giller, S. Becker, M. Baldus and A. Lange, High resolution observed in 800 MHz DNP spectra of extremely rigid type III secretion needles, *J. Biomol. NMR*, 2016, **65**, 121–126.

16 W. Y. Chow, B. P. Norman, N. B. Roberts, L. R. Ranganath, C. Teutloff, R. Bittl, M. J. Duer, J. A. Gallagher and H. Oschkinat, Pigmentation Chemistry and Radical-Based Collagen Degradation in Alkaptonuria and Osteoarthritic Cartilage, *Angew. Chem., Int. Ed.*, 2020, **59**, 11937–11942.

17 R. W. Hooper, B. A. Klein and V. K. Michaelis, Dynamic Nuclear Polarization (DNP) 101: A New Era for Materials, *Chem. Mater.*, 2020, **32**, 4425–4430.

18 F. A. Perras, T. Kobayashi and M. Pruski, Growing Signals from the Noise: Challenging Nuclei in Materials DNP, *eMagRes*, 2018, vol. 7, pp. 35–50.

19 T. Wolf, S. Kumar, H. Singh, T. Chakrabarty, F. Aussenac, A. I. Frenkel, D. T. Major and M. Leskes, Endogenous Dynamic Nuclear Polarization for Natural Abundance 17 O and Lithium NMR in the Bulk of Inorganic Solids, *J. Am. Chem. Soc.*, 2019, **141**, 451–462.

20 P. Berruyer, L. Emsley and A. Lesage, in *eMagRes*, John Wiley & Sons, Ltd, 2018, pp. 93–104.

21 T. V. Can, M. a. Caporini, F. Mentink-Vigier, B. Corzilius, J. J. Walish, M. Rosay, W. E. Maas, M. Baldus, S. Vega, T. M. Swager and R. G. Griffin, Overhauser effects in insulating solids, *J. Chem. Phys.*, 2014, **141**, 064202.

22 F. Mentink-Vigier, U. Akbey, Y. Hovav, S. Vega, H. Oschkinat and A. Feintuch, Fast passage dynamic nuclear polarization on rotating solids, *J. Magn. Reson.*, 2012, **224**, 13–21.

23 K. R. Thurber and R. Tycko, Theory for cross effect dynamic nuclear polarization under magic-angle spinning in solid state nuclear magnetic resonance: The importance of level crossings, *J. Chem. Phys.*, 2012, **137**, 084508.

24 T. V. Can, Q. Z. Ni and R. G. Griffin, Mechanisms of dynamic nuclear polarization in insulating solids, *J. Magn. Reson.*, 2015, **253**, 23–35.

25 K.-N. Hu, G. T. Debelouchina, A. A. Smith and R. G. Griffin, Quantum mechanical theory of dynamic nuclear polarization in solid dielectrics, *J. Chem. Phys.*, 2011, **134**, 125105.

26 F. Mentink-Vigier, Numerical recipes for faster MAS-DNP simulations, *J. Magn. Reson.*, 2021, **333**, 107106.

27 K.-N. Hu, V. S. Bajaj, M. Rosay and R. G. Griffin, High-frequency dynamic nuclear polarization using mixtures of TEMPO and trityl radicals, *J. Chem. Phys.*, 2007, **126**, 044512.

28 C. Sauvée, M. Rosay, G. Casano, F. Aussenac, R. T. Weber, O. Ouari and P. Tordo, Highly Efficient, Water-Soluble Polarizing Agents for Dynamic Nuclear Polarization at High Frequency, *Angew. Chem., Int. Ed.*, 2013, **52**, 10858–10861.

29 A. Zagdoun, G. Casano, O. Ouari, M. Schwarzwälder, A. J. Rossini, F. Aussenac, M. Yulikov, G. Jeschke, C. Copéret, A. Lesage, P. Tordo and L. Emsley, Large molecular weight nitroxide biradicals providing efficient dynamic nuclear polarization at temperatures up to 200 K, *J. Am. Chem. Soc.*, 2013, **135**, 12790–12797.

Open Access Article. Published on 13 March 2023. Downloaded on 2/7/2026 7:50:00 PM. This article is licensed under a Creative Commons Attribution-NonCommercial 3.0 Unported Licence.

30 A. P. Jagtap, M.-A. Geiger, D. Stöppler, M. Orwick-Rydmark, H. Oschkinat and S. T. Sigurdsson, bcTol: a highly water-soluble biradical for efficient dynamic nuclear polarization of biomolecules, *Chem. Commun.*, 2016, **52**, 7020–7023.

31 M. A. Geiger, A. P. Jagtap, M. Kaushik, H. Sun, D. Stöppler, S. T. Sigurdsson, B. Corzilius and H. Oschkinat, Efficiency of Water-Soluble Nitroxide Biradicals for Dynamic Nuclear Polarization in Rotating Solids at 9.4 T: bcTol-M and cyolyl-TOTAPOL as New Polarizing Agents, *Chem. – Eur. J.*, 2018, **24**, 13485–13494.

32 A. Lund, G. Casano, G. Menzildjian, M. Kaushik, G. Stevanato, M. Yulikov, R. Jabbour, D. Wisser, M. Renom-Carrasco, C. Thieuleux, F. Bernada, H. Karoui, D. Siri, M. Rosay, I. V. Sergeyev, D. Gajan, M. Lelli, L. Emsley, O. Ouari and A. Lesage, TinyPols: A family of water-soluble binitroxides tailored for dynamic nuclear polarization enhanced NMR spectroscopy at 18.8 and 21.1 T, *Chem. Sci.*, 2020, **11**, 2810–2818.

33 F. Mentink-Vigier, I. Marin-Montesinos, A. P. Jagtap, T. Halbritter, J. van Tol, S. Hediger, D. Lee, S. T. Sigurdsson and G. De Paepe, Computationally Assisted Design of Polarizing Agents for Dynamic Nuclear Polarization Enhanced NMR: The AsymPol Family, *J. Am. Chem. Soc.*, 2018, **140**, 11013–11019.

34 R. Harrabi, T. Halbritter, F. Aussenac, O. Dakhlaoui, J. van Tol, K. K. Damodaran, D. Lee, S. Paul, S. Hediger, F. Mentink-Vigier, S. Th. Sigurdsson and G. De Paëpe, Highly Efficient Polarizing Agents for MAS-DNP of Proton-Dense Molecular Solids, *Angew. Chem., Int. Ed.*, 2022, DOI: 10.1002/anie.202114103.

35 G. Mathies, M. A. Caporini, V. K. Michaelis, Y. Liu, K.-N. Hu, D. Mance, J. L. Zweier, M. Rosay, M. Baldus and R. G. Griffin, Efficient Dynamic Nuclear Polarization at 800 MHz/527 GHz with Trityl-Nitroxide Biradicals, *Angew. Chem.*, 2015, **127**, 11936–11940.

36 F. Mentink-Vigier, G. Mathies, Y. Liu, A.-L. Barra, M. A. Caporini, D. Lee, S. Hediger, R. G. Griffin and G. De Paëpe, Efficient cross-effect dynamic nuclear polarization without depolarization in high-resolution MAS NMR, *Chem. Sci.*, 2017, **8**, 8150–8163.

37 D. Wisser, G. Karthikeyan, A. Lund, G. Casano, H. Karoui, M. Yulikov, G. Menzildjian, A. C. Pinon, A. Purea, F. Engelke, S. R. Chaudhari, D. Kubicki, A. J. Rossini, I. B. Moroz, D. Gajan, C. Copéret, G. Jeschke, M. Lelli, L. Emsley, A. Lesage and O. Ouari, BDPA-Nitroxide Biradicals Tailored for Efficient Dynamic Nuclear Polarization Enhanced Solid-State NMR at Magnetic Fields up to 21.1 T, *J. Am. Chem. Soc.*, 2018, **140**, 13340–13349.

38 D. Mance, P. Gast, M. Huber, M. Baldus and K. L. Ivanov, The magnetic field dependence of cross-effect dynamic nuclear polarization under magic angle spinning, *J. Chem. Phys.*, 2015, **142**, 234201.

39 F. Mentink-Vigier, U. Akbey, H. Oschkinat, S. Vega and A. Feintuch, Theoretical aspects of Magic Angle Spinning - Dynamic Nuclear Polarization, *J. Magn. Reson.*, 2015, **258**, 102–120.

40 F. Mentink-Vigier, S. Vega and G. De Paepe, Fast and accurate MAS–DNP simulations of large spin ensembles, *Phys. Chem. Chem. Phys.*, 2017, **19**, 3506–3522.

41 F. Mentink-Vigier, Optimizing nitroxide biradicals for cross-effect MAS-DNP: the role of g-tensors' distance, *Phys. Chem. Chem. Phys.*, 2020, **22**, 3643–3652.

42 A. Equbal, K. Tagami and S. Han, Balancing dipolar and exchange coupling in biradicals to maximize cross effect dynamic nuclear polarization, *Phys. Chem. Chem. Phys.*, 2020, **22**, 13569–13579.

43 W. Zhai, A. Lucini Paioni, X. Cai, S. Narasimhan, J. Medeiros-Silva, W. Zhang, A. Rockenbauer, M. Weingarth, Y. Song, M. Baldus and Y. Liu, Postmodification via Thiol-Click Chemistry Yields Hydrophilic Trityl-Nitroxide Biradicals for Biomolecular High-Field Dynamic Nuclear Polarization, *J. Phys. Chem. B*, 2020, **124**, 9047–9060.

44 X. Cai, A. Lucini Paioni, A. Adler, R. Yao, W. Zhang, D. Beriashvili, A. Safeer, A. Gurinov, A. Rockenbauer, Y. Song, M. Baldus and Y. Liu, Highly Efficient Trityl-Nitroxide Biradicals for Biomolecular High-Field Dynamic Nuclear Polarization, *Chem. – Eur. J.*, 2021, **27**, 12758–12762.

45 P. Berruyer, S. Björgvinsdóttir, A. Bertarello, G. Stevanato, Y. Rao, G. Karthikeyan, G. Casano, O. Ouari, M. Lelli, C. Reiter, F. Engelke and L. Emsley, Dynamic Nuclear Polarization Enhancement of 200 at 21.15 T Enabled by 65 kHz Magic Angle Spinning, *J. Phys. Chem. Lett.*, 2020, **11**, 8386–8391.

46 E. L. Dane, T. Maly, G. T. Debelouchina, R. G. Griffin and T. M. Swager, Synthesis of a BDPA-TEMPO biradical, *Org. Lett.*, 2009, **11**, 1871–1874.

47 S. Mandal and S. Th. Sigurdsson, On the Limited Stability of BDPA Radicals, *Chem. – Eur. J.*, 2020, **26**, 7486–7491.

48 S. Mandal and S. Th. Sigurdsson, Water-soluble BDPA radicals with improved persistence, *Chem. Commun.*, 2020, **56**, 13121–13124.

49 P. Berruyer, A. Bertarello, S. Björgvinsdóttir, M. Lelli and L. Emsley, 1H Detected Relayed Dynamic Nuclear Polarization, *J. Phys. Chem. C*, 2022, **126**, 7564–7570.

50 K. Sato, R. Hirao, I. Timofeev, O. Krumkacheva, E. Zaytseva, O. Rogozhnikova, V. M. Tormyshev, D. Trukhin, E. Bagryanskaya, T. Gutmann, V. Klimavicius, G. Buntkowsky, K. Sugisaki, S. Nakazawa, H. Matsuoka, K. Toyota, D. Shiomi and T. Takui, Trityl-Aryl-Nitroxide-Based Genuinely g -Engineered Biradicals, As Studied by Dynamic Nuclear Polarization, Multifrequency ESR/ENDOR, Arbitrary Wave Generator Pulse Microwave Waveform Spectroscopy, and Quantum Chemical Calculations, *J. Phys. Chem. A*, 2019, **123**, 7507–7517.

51 S. Bothe, J. Nowag, V. Klimavičius, M. Hoffmann, T. I. Troitskaya, E. V Amosov, V. M. Tormyshev, I. Kirilyuk, A. Taratayko, A. Kuzhelev, D. Parkhomenko, E. Bagryanskaya, T. Gutmann and G. Buntkowsky, Novel Biradicals for Direct Excitation Highfield Dynamic Nuclear Polarization, *J. Phys. Chem. C*, 2018, **122**, 11422–11432.

52 D. J. Kubicki, G. Casano, M. Schwarzwälder, S. Abel, C. Sauvée, K. Ganesan, M. Yulikov, A. J. Rossini,

 © 2023 The Author(s). Published by the Royal Society of Chemistry

Open Access Article. Published on 13 March 2023. Downloaded on 2/7/2026 7:50:00 PM.
This article is licensed under a Creative Commons Attribution-NonCommercial 3.0 Unported Licence.

G. Jeschke, C. Copéret, A. Lesage, P. Tordo, O. Ouari and L. Emsley, Rational design of dinitroxide biradicals for efficient cross-effect dynamic nuclear polarization, *Chem. Sci.*, 2016, **7**, 550–558.

53 C. Sauvée, G. Casano, S. Abel, A. Rockenbauer, D. Akhmetzyanov, H. Karoui, D. Siri, F. Aussenac, W. Maas, R. T. Weber, T. F. Prisner, M. Rosay, P. Tordo and O. Ouari, Tailoring of Polarizing Agents in the bTurea Series for Cross-Effect Dynamic Nuclear Polarization in Aqueous Media, *Chem. – Eur. J.*, 2016, **22**, 5598–5606.

54 G. Stevanato, G. Casano, D. J. Kubicki, Y. Rao, L. E. Hofer, G. Menzildjian, H. Karoui, D. Siri, M. Cordova, M. Yulikov, G. Jeschke, M. Lelli, A. Lesage, O. Ouari and L. Emsley, Open and closed radicals: Local geometry around unpaired electrons governs magic-angle spinning dynamic nuclear polarization performance, *J. Am. Chem. Soc.*, 2020, **142**, 16587–16599.

55 F. A. Perras, R. R. Reinig, I. I. Slowing, A. D. Sadow and M. Pruski, Effects of Biradical Deuteration on the Performance of DNP: Towards Better Performing Polarizing Agents, *Phys. Chem. Chem. Phys.*, 2015, **18**, 65–69.

56 F. Mentink-Vigier, A.-L. Barra, J. van Tol, S. Hediger, D. Lee and G. De Paepe, De novo prediction of cross-effect efficiency for magic angle spinning dynamic nuclear polarization, *Phys. Chem. Chem. Phys.*, 2019, **21**, 2166–2176.

57 F. Mentink-Vigier, T. Dubroca, J. van Tol and S. T. Sigurdsson, The distance between g-tensors of nitroxide biradicals governs MAS-DNP performance: The case of the bTurea family, *J. Magn. Reson.*, 2021, **329**, 107026.

58 S. R. Chaudhari, P. Berruyer, D. Gajan, C. Reiter, F. Engelke, D. L. Silverio, C. Copéret, M. Lelli, A. Lesage and L. Emsley, Dynamic nuclear polarization at 40 kHz magic angle spinning, *Phys. Chem. Chem. Phys.*, 2016, **18**, 10616–10622.

59 H. Takahashi, C. Fernández-de-Alba, D. Lee, V. Maurel, S. Gambarelli, M. Bardet, S. Hediger, A. L. Barra and G. De Paepe, Optimization of an absolute sensitivity in a glassy matrix during DNP-enhanced multidimensional solid-state NMR experiments, *J. Magn. Reson.*, 2014, **239**, 91–99.

60 F. J. Scott, T. Dubroca, F. Mentink-Vigier and J. R. Long, in *Experimental NMR Conference*, Orlando, Florida, United States, 2022.

61 W. Moore, R. Yao, Y. Liu, S. S. Eaton and G. R. Eaton, Spin-spin interaction and relaxation in two trityl-nitroxide diradicals, *J. Magn. Reson.*, 2021, **332**, 107078.

62 T. J. Reddy, T. Iwama, H. J. Halpern and V. H. Rawal, General Synthesis of Persistent Trityl Radicals for EPR Imaging of Biological Systems, *J. Org. Chem.*, 2002, **67**, 4635–4639.

63 A. A. Bobko, I. Dhimitruka, J. L. Zweier and V. V. Khramtsov, Trityl radicals as persistent dual function pH and oxygen probes for in vivo electron paramagnetic resonance spectroscopy and imaging: Concept and experiment, *J. Am. Chem. Soc.*, 2007, **129**, 7240–7241.

64 H. Sato, V. Kathirvelu, A. Fielding, J. P. Blinco, A. S. Micallef, S. E. Bottle, S. S. Eaton and G. R. Eaton, Impact of molecular size on electron spin relaxation rates of nitroxyl radicals in glassy solvents between 100 and 300 K, *Mol. Phys.*, 2007, **105**, 2137–2151.

65 H. Chen, A. G. Maryasov, O. Yu. Rogozhnikova, D. V. Trukhin, V. M. Tormyshev and M. K. Bowman, Electron spin dynamics and spin–lattice relaxation of trityl radicals in frozen solutions, *Phys. Chem. Chem. Phys.*, 2016, **18**, 24954–24965.

66 A. Lunghi, Spin-Phonon Relaxation in Magnetic Molecules: Theory, Predictions and Insights, *arXiv*, 2022, preprint, arXiv:2202.03776, DOI: 10.48550/arXiv.2202.03776.

67 A. Lunghi, Toward exact predictions of spin-phonon relaxation times: An ab initio implementation of open quantum systems theory, *Sci. Adv.*, 2022, **8**, 1–11.

68 T. Dubroca, A. N. A. N. Smith, K. J. K. J. Pike, S. Froud, R. Wylde, B. Trociewitz, J. E. McKay, F. Mentink-Vigier, J. van Tol, S. Wi, W. W. Brey, J. R. Long, L. Frydman and S. Hill, A quasi-optical and corrugated waveguide microwave transmission system for simultaneous dynamic nuclear polarization NMR on two separate 14.1 T spectrometers, *J. Magn. Reson.*, 2018, **289**, 35–44.

69 M. Rosay, M. Blank and F. Engelke, Instrumentation for solid-state dynamic nuclear polarization with magic angle spinning NMR, *J. Magn. Reson.*, 2016, **264**, 88–98.

70 I. V. Sergeyev, F. Aussenac, A. Purea, C. Reiter, E. Bryerton, S. Retzloff, J. Hesler, L. Tometich and M. Rosay, Efficient 263 GHz magic angle spinning DNP at 100 K using solid-state diode sources, *Solid State Nucl. Magn. Reson.*, 2019, **100**, 63–69.

71 M. Blank and K. L. Felch, Millimeter-wave Sources for DNP-NMR, *eMagRes*, 2018, vol. 7, pp. 155–166.

72 K. R. Thurber and R. Tycko, Low-temperature dynamic nuclear polarization with helium-cooled samples and nitrogen-driven magic-angle spinning, *J. Magn. Reson.*, 2016, **264**, 99–106.

73 T. F. Kemp, H. R. W. Dannatt, N. S. Barrow, A. Watts, S. P. Brown, M. E. Newton and R. Dupree, Dynamic Nuclear Polarization enhanced NMR at 187 GHz/284 MHz using an Extended Interaction Klystron amplifier, *J. Magn. Reson.*, 2016, **265**, 77–82.

74 K. R. Thurber, A. Potapov, W. M. Yau and R. Tycko, Solid state nuclear magnetic resonance with magic-angle spinning and dynamic nuclear polarization below 25 K, *J. Magn. Reson.*, 2013, **226**, 100–106.

75 T. A. Siaw, A. Leavesley, A. Lund, I. Kaminker and S. Han, A versatile and modular quasi optics-based 200 GHz dual dynamic nuclear polarization and electron paramagnetic resonance instrument, *J. Magn. Reson.*, 2016, **264**, 131–153.

76 M. P. Hanrahan, Y. Chen, R. Blome-Fernández, J. L. Stein, G. F. Pach, M. A. S. Adamson, N. R. Neale, B. M. Cossairt, J. Vela and A. J. Rossini, Probing the Surface Structure of Semiconductor Nanoparticles by DNP SENS with Dielectric Support Materials, *J. Am. Chem. Soc.*, 2019, **141**, 15532–15546.

77 D. J. Kubicki, A. J. Rossini, A. Purea, A. Zagdoun, O. Ouari, P. Tordo, F. Engelke, A. Lesage and L. Emsley, Amplifying dynamic nuclear polarization of frozen solutions by incorporating dielectric particles, *J. Am. Chem. Soc.*, 2014, **136**, 15711–15718.

Open Access Article. Published on 13 March 2023. Downloaded on 2/7/2026 7:50:00 PM.
This article is licensed under a Creative Commons Attribution-NonCommercial 3.0 Unported Licence.

78 S. Bothe, J. Nowag, V. Klimavičius, M. Hoffmann, T. I. Troitskaya, E. V. Amosov, V. M. Tormyshev, I. Kirilyuk, A. Taratayko, A. Kuzhelev, D. Parkhomenko, E. Bagryanskaya, T. Gutmann and G. Buntkowsky, Novel Biradicals for Direct Excitation Highfield Dynamic Nuclear Polarization, *J. Phys. Chem. C*, 2018, **122**, 11422–11432.

79 Y. Li, A. Equbal, K. Tagami and S. Han, Electron spin density matching for cross-effect dynamic nuclear polarization, *Chem. Commun.*, 2019, **55**, 7591–7594.

80 K. R. Thurber and R. Tycko, Perturbation of nuclear spin polarizations in solid state NMR of nitroxide-doped samples by magic-angle spinning without microwaves, *J. Chem. Phys.*, 2014, **140**, 184201.

81 F. Mentink-Vigier, S. Paul, D. Lee, A. Feintuch, S. Hediger, S. Vega and G. De Paëpe, Nuclear depolarization and absolute sensitivity in magic-angle spinning cross effect dynamic nuclear polarization, *Phys. Chem. Chem. Phys.*, 2015, **17**, 21824–21836.

82 F. A. Perras, S. L. Carnahan, W.-S. Lo, C. J. Ward, J. Yu, W. Huang and A. J. Rossini, Hybrid quantum-classical simulations of magic angle spinning dynamic nuclear polarization in very large spin systems, *J. Chem. Phys.*, 2022, **156**, 124112.

83 S. R. Chaudhari, D. Wisser, A. C. Pinon, P. Berruyer, D. Gajan, P. Tordo, O. Ouari, C. Reiter, F. Engelke, C. Copéret, M. Lelli, A. Lesage and L. Emsley, Dynamic Nuclear Polarization Efficiency Increased by Very Fast Magic Angle Spinning, *J. Am. Chem. Soc.*, 2017, **139**, 10609–10612.

84 A. Lesage, M. Lelli, D. Gajan, M. A. Caporini, V. Vitzthum, P. Miéville, J. Alauzun, A. Roussey, C. Thieuleux, A. Mehdi, G. Bodenhausen, C. Copéret and L. Emsley, Surface enhanced NMR spectroscopy by dynamic nuclear polarization, *J. Am. Chem. Soc.*, 2010, **132**, 15459–15461.

85 A. Zagdoun, G. Casano, O. Ouari, G. Lapadula, A. J. Rossini, M. Lelli, M. Baffert, D. Gajan, L. Veyre, W. E. Maas, M. Rosay, R. T. Weber, C. Thieuleux, C. Coperet, A. Lesage, P. Tordo and L. Emsley, A slowly relaxing rigid biradical for efficient dynamic nuclear polarization surface-enhanced NMR spectroscopy: Expeditious characterization of functional group manipulation in hybrid materials, *J. Am. Chem. Soc.*, 2012, **134**, 2284–2291.

86 O. Lafon, A. S. L. Thankamony, T. Kobayashi, D. Carnevale, V. Vitzthum, I. I. Slowing, K. Kandel, H. Vezin, J. P. Amoureux, G. Bodenhausen and M. Pruski, Mesoporous silica nanoparticles loaded with surfactant: Low temperature magic angle spinning 13C and 29Si NMR enhanced by dynamic nuclear polarization, *J. Phys. Chem. C*, 2013, **117**, 1375–1382.

87 M. Lelli, D. Gajan, A. Lesage, M. A. Caporini, V. Vitzthum, P. Miéville, F. Héroguel, F. Rascón, A. Roussey, C. Thieuleux, M. Boualleg, L. Veyre, G. Bodenhausen, C. Copéret and L. Emsley, Fast characterization of functionalized silica materials by silicon-29 surface-enhanced NMR spectroscopy using dynamic nuclear polarization, *J. Am. Chem. Soc.*, 2011, **133**, 2104–2107.

88 V. Vitzthum, P. Miéville, D. Carnevale, M. A. Caporini, D. Gajan, C. Copéret, M. Lelli, A. Zagdoun, A. J. Rossini, A. Lesage, L. Emsley and G. Bodenhausen, Dynamic nuclear polarization of quadrupolar nuclei using cross polarization from protons: Surface-enhanced aluminium-27 NMR, *Chem. Commun.*, 2012, **48**, 1988–1990.

89 D. Lee, H. Takahashi, A. S. L. Thankamony, J.-P. Dacquin, M. Bardet, O. Lafon and G. De Paëpe, Enhanced Solid-State NMR Correlation Spectroscopy of Quadrupolar Nuclei Using Dynamic Nuclear Polarization, *J. Am. Chem. Soc.*, 2012, **134**, 18491–18494.

90 D. Lee, N. T. Duong, O. Lafon and G. De Paepe, Primostrato Solid-State NMR Enhanced by Dynamic Nuclear Polarization: Pentacoordinated Al3+ Ions Are Only Located at the Surface of Hydrated γ-Alumina, *J. Phys. Chem. C*, 2014, **118**, 25065–25076.

91 L. Frydman and J. S. Harwood, Isotropic Spectra of Half-Integer Quadrupolar Spins from Bidimensional Magic-Angle Spinning NMR, *J. Am. Chem. Soc.*, 1995, **117**, 5367–5368.

92 A. Medek, J. S. Harwood and L. Frydman, Multiple-Quantum Magic-Angle Spinning NMR: A New Method for the Study of Quadrupolar Nuclei in Solids, *J. Am. Chem. Soc.*, 1995, **117**, 12779–12787.

93 R. Yao, D. Beriashvili, W. Zhang, S. Li, A. Safeer, A. Gurinov, A. Rockenbauer, Y. Yang, Y. Song, M. Baldus and Y. Liu, Highly bioresistant, hydrophilic and rigidly linked trityl-nitroxide biradicals for cellular high-field dynamic nuclear polarization, *Chem. Sci.*, 2022, **13**, 14157–14164.

94 L. Delage-Laurin, R. S. Palani, N. Golota, M. Mardini, Y. Ouyang, K. O. Tan, T. M. Swager and R. G. Griffin, Overhauser Dynamic Nuclear Polarization with Selectively Deuterated BDPA Radicals, *J. Am. Chem. Soc.*, 2021, **143**, 20281–20290.

 © 2023 The Author(s). Published by the Royal Society of Chemistry